International Journal of
Environmental Research and Public Health

MDPI

Article

Adsorption Performance of Cd(II) by Chitosan-Fe_3O_4-Modified Fish Bone Char

Wenhao Yang [1,2,3,†], Wenwen Luo [1,2,†], Tong Sun [1,2], Yingming Xu [1,2] and Yuebing Sun [1,2,*]

[1] Key Laboratory of Original Environmental Pollution Prevention and Control, Ministry of Agriculture and Rural Affairs, Tianjin 300191, China; 18865712611@163.com (W.Y.); 17602669062@163.com (W.L.); 17862685017@163.com (T.S.); xuyingming@aepi.org.cn (Y.X.)
[2] Tianjin Key Laboratory of Agro-Environment and Agro-Products, Agro-Environmental Protection Institute, Ministry of Agriculture and Rural Affairs, Tianjin 300191, China
[3] College of Resources and Environment, Northeast Agricultural University, Harbin 150030, China
* Correspondence: sunyuebing@aepi.org.cn or sunyuebing2008@126.com
† These authors contributed equally to this work.

Abstract: In order to develop a low-cost, fast, and efficient adsorbent, the fish bone charcoal B_{600} prepared at 600 °C was modified by chitosan (Cs) and Fe_3O_4 to produce the material Cs-Fe_3O_4-B_{600}. Results showed that Cs-Fe_3O_4-B_{600} had magnetic responsiveness and can achieve solid–liquid separation, macropores disappeared, pore volume and specific surface area are increased, and amino functional groups appear on the surface. The adsorption process of Cd(II) by Cs-Fe_3O_4-B_{600} conformed best to the pseudo-second order kinetics model and the Langmuir model, respectively. The behavior over a whole range of adsorption was consistent with chemical adsorption being the rate-controlling step, which is a very fast adsorption process, and the isothermal adsorption is mainly monolayer adsorption, which belongs to favorable adsorption. In addition, the saturated adsorption capacity obtained for the Cs-Fe_3O_4-B_{600} to Cd(II) was 64.31 $mg \cdot g^{-1}$, which was 1.7 times than B_{600}. The structure and morphology of Cs-Fe_3O_4-B_{600} were characterized through SEM-EDS, TEM, FTIR, and XRD, indicating that the main mechanism of Cs-Fe_3O_4-B_{600} and Cd(II) is mainly the complexation of amino groups, and it also includes part of the ion exchange between Cd(II) and Fe_3O_4. Therefore, Cs-Fe_3O_4-B_{600} can be employed as an effective agent for remediation of Cd contaminated water.

Keywords: Cd; fish bone char; Fe_3O_4; chitosan; modification; adsorption mechanism

Citation: Yang, W.; Luo, W.; Sun, T.; Xu, Y.; Sun, Y. Adsorption Performance of Cd(II) by Chitosan-Fe_3O_4-Modified Fish Bone Char. *Int. J. Environ. Res. Public Health* **2022**, *19*, 1260. https://doi.org/10.3390/ijerph19031260

Academic Editor: Paul B. Tchounwou

Received: 12 December 2021
Accepted: 20 January 2022
Published: 23 January 2022

1. Introduction

Cadmium (Cd) is a highly toxic carcinogen, which enters the human body through the food chain and causes damage to human health [1,2]. Human intake of Cd mainly includes food, smoking, and drinking water. Among them, grains and vegetables are the largest sources of human long-term intake of Cd [3]. Cd in the soil is easily absorbed by plants and transported in their tissues [4]. At present, Cd content of many food crops in China has exceeded the corresponding national food safety standard [3,5]. Wastewater irrigation is an important cause of cadmium pollution in agricultural soil. Therefore, it is very important to remove cadmium in wastewater.

Cd pollution cannot reduce or even eliminate its harmfulness through environmental self-purification but can only achieve the transformation of the occurrence state and the migration of the location. A variety of remediation measures are used for the remediation of Cd-contaminated soils, such as physical and chemical remediation, microbial remediation, and phytoremediation [6]. Currently, the adsorption method has attracted much attention due to its high efficiency, low cost, and non-secondary pollution. Adsorption is considered to be a process in which molecules gather from a fluid to a solid surface. In recent years, the use of low-cost, widely sourced industrial/agricultural/domestic waste or

by-products as adsorbents to remove heavy metals in water bodies has received widespread attention [7–10]. Bone char mainly includes hydroxyapatite (70–76%), a small part of char (9–11%) and carbonate (7–9%) [11]. Several studies have demonstrated that bone char has a good adsorption effect on heavy metals Cu(II), Zn(II), Co(II), Hg(II) [12–14]. For example, the research of Wang [15] and Liu [16] showed that bone char also has a good treatment effect on Pb(II) and As(V), and the adsorption capacity can reach 84.75 and 0.335 $mg \cdot g^{-1}$, respectively. In addition, Moreno et al. [17] found that the saturated adsorption capacity of bone char for Mn and Ni can reach 29.56 and 35.44 $mg \cdot g^{-1}$, respectively. Sneddon et al. [18] used column leaching experiments to study the fixation effect of bone char on Pb(II), Zn(II), and Cd(II) in soil, that is, to test the stability of metals in contaminated soil by forming low-soluble metal phosphates. The results show that when bone char:soil = 1:10 (mass ratio), the release of heavy metals is inhibited during the whole process of the experiment, which may involve surface complexation and ion exchange.

The modification of bone meal materials usually refers to the use of impregnation or co-precipitation methods to load target functional groups or target components on the surface of the material. Common composite modifications include metal ion loading modification such as aluminum, iron, lanthanum, sulfhydryl, and other surface group loading modification, graphene modification, γ-Fe_2O_3, Fe_3O_4, $NiFe_2O_4$, $CoFe_2O_4$, $CuFe_2O_4$, and $ZnFe_2O_4$ particles and other magnetic properties modified [19–24]. However, compared with bone meal, bone char materials have well-developed pores and are more suitable as a carrier for loading materials. Therefore, the composite modification of bone meal materials is mostly performed on the bone char obtained by treatment at different temperatures.

Studies have shown that magnetic materials not only easily achieve solid–liquid separation, but also have a good removal effect on heavy metals. For example, functionalized magnetic microspheres $NiFe_2O_4$ can adsorb Cu up to 20.16 $mg \cdot g^{-1}$ [25], FeS-coated iron can adsorb Cr(VI) up to 69.7 $mg \cdot g^{-1}$ [26], $FeNi_3/TiO_2$ material can adsorb Cr(VI) up to 76.335 $mg \cdot g^{-1}$ [27]. Among the above-mentioned magnetic particles, Fe_3O_4 is widely used because of its strong superparamagnetism, low toxicity, and easy synthesis [28,29]. The typical synthesis process of nano Fe_3O_4 particles mainly includes DC (Direct Current) arc plasma method, thermal decomposition method, co-precipitation method, hydrothermal method, and microemulsion method. Du et al. [30] used the co-precipitation method to prepare Fe_3O_4 magnetic biochar and applied it to the treatment of heavy-metal polluted wastewater. The results show that after the magnetic modification, the specific surface area of the adsorbent increases, and the removal rate of Cu and Zn can reach 61.1% and 60.4%, respectively. During the modification process, functional groups such as hydroxyl and carboxyl groups increased [30]. Hu et al. [31] studied the removal of Cd(II) by magnetically modified corn stalk biochar, and the results showed that after the material was magnetically modified, the pH value, specific surface area, and polar oxygen-containing functional groups all increased, resulting in a saturated adsorption capacity. The mechanism of magnetic biochar to remove Cd is ion exchange, surface complexation, electrostatic adsorption, and cation-π interaction. The strong affinity of iron oxide for Cd can enhance the complexation between them [31]. In addition, chitosan is a low cost, biodegradable, and nontoxic biopolymer [32]. Chitosan has a large number of amino functional groups and has strong adsorption capacity for heavy metals in aqueous solution, so it can be widely used in the removal of heavy metal pollutants [33]. However, due to the low specific surface area and limited active sites of chitosan, its adsorption capacity is still insufficient [34]. Chitosan can be introduced on the surface of fish bone char to enhance the adsorption capacity and active sites of fish bone char for heavy metals [34].

However, there are few studies on the effect and mechanism of chitosan and Fe_3O_4 composite modified bone char for Cd removal. In this work, we successfully prepared a novel chitosan combined Fe_3O_4 modified fish bone char (Cs-Fe_3O_4-B_{600}), which can be used as a suitable adsorbent for cadmium solution. The objectives of this study were to (1) prepare and characterize the Cs-Fe_3O_4-B_{600} and (2) explore the capabilities and mechanisms of Cs-Fe_3O_4-B_{600} for adsorption on Cd.

2. Materials and Methods

2.1. Adsorbent Preparation

2.1.1. Preparation of Fish Bone Char

The fish bone meal used in the experiment was pulverized by a universal pulverizer and passed through a 100-mesh sieve. A part of the sieved fish bone meal was selected, and N_2 was used as a protective gas to react in a muffle furnace (SLX1100-50, Shanghai Shengli Testing Instrument Co., Ltd., Shanghai, China) at 200, 400, 600, and 800 °C for 3.5 h to obtain fish bone char treated at different temperatures. By measuring the Cd adsorption capacity of fish bone char prepared at different temperatures, we found that fish bone char prepared at 600 °C (B_{600}) had the highest adsorption capacity, so B_{600} was selected for subsequent experiments. B_{600} was grind pulverized and passed through a 200-mesh sieve for use. In addition, the basic properties of fish bone meal are as follows. The main component of fish bone meal is $Ca_{10}(PO_4)_6(OH)_2$, the specific surface area is 2.27 $m^2 \cdot g^{-1}$, the pore volume is 0.0035 $cm^3 \cdot g^{-1}$, and the average pore diameter is 4.811 nm.

2.1.2. Preparation of Nano Fe_3O_4

The ultrapure water was boiled and then cooled and sealed for later use. After ferrous chloride tetrahydrate (0.0994 g, Shanghai Macklin Biochemical Co., Ltd., Shanghai, China) and ferric chloride hexahydrate (2.7029 g, Shanghai Macklin Biochemical Co., Ltd., Shanghai, China) were dissolved in the above ultrapure water (100 mL) in a three-necked flask, ammonia water with a concentration of 3.5 M was added dropwise, and then vigorously stirred with a Vortex Mixer (QL-866, Haimen Kylin-Bell Lab Instruments Co., Ltd., Haimen, China) to mix well and when the measured pH was 10, addition of ammonia water (about 40 mL) was stopped. In this process, the nitrogen-blowing device (N-EVAP, Organomation, Berlin, MA, USA) was used to pass N_2 to undertake the reaction under anaerobic conditions. The obtained precipitate was washed with deionized water and dried in a muffle furnace at 70 °C. The above process was repeated several times to obtain a sufficient amount of nano Fe_3O_4.

2.1.3. Preparation of Chitosan-Fe_3O_4-Modified Fish Bone Char

Chitosan (100 g, Shanghai Macklin Biochemical Co., Ltd., Shanghai, China) was added to absolute ethanol (1000 mL) and stirred vigorously for 2 h to obtain a viscous gum. Bone char (5 g) (B_{600}, 200-mesh sieve) and nano Fe_3O_4 (2 g) were added to the above viscous gel, and the Vortex Mixer was vigorously stirred for 1 h. The above homogeneous mixture was added dropwise to 500 mL 15% NaOH and 95% absolute ethanol mixture (volume ratio 4:1) with a rubber tip dropper, and continuously stirred to produce chitosan-Fe_3O_4-modified fish bone char mixture. After keeping in the solution for 12 h, the precipitate was collected, washed with deionized water to remove surface impurities, dried in a muffle furnace at 70 °C, and sieved for later use. The resulting material was recorded as Cs-Fe_3O_4-B_{600}. This method refers to Reza's magnetic modification of bone char [35] and optimizes it on this basis.

2.2. Characterization

The magnetic properties of Cs-Fe_3O_4-B_{600} were characterized by a Vibrating Sample Magnetometer (Mpms Squid, American quantum design company, San Diego, CA, USA) at room temperature, applying a magnetic field of −20 kOe–20 kOe; the specific surface area and pore volume of Cs-Fe_3O_4-B_{600} were measured by a specific surface area analyzer (Quadrasorb Si, Quanta Instruments, Inc., Boynton Beach, FL, USA) using multipoint BET (Method of Brunauer, Emmett and Teller) method and BJH (Method of Barrett, Joyner and Halenda). The multifunctional X-ray diffractometer (Bruker D8 Advance, Bruker, Karlsruhe, Germany) was used to perform XRD (diffraction of x-rays) analysis on Cs-Fe_3O_4-B_{600}, with a scan range of 10°–90°, a scan rate of 4°·cm^{-1}, and a scan step size of 0.02°; Fourier transform infrared spectrometer (Thermo Nicolet 380, Madison, WI, USA) was used for FTIR (Fourier Transform Infrared Spectrometer) analysis of Cs-Fe_3O_4-B_{600}; The measured

wavenumber range was 400–4000 cm^{-1} and the resolution was 1 cm^{-1}; Scanning electron microscope (Hitachi SU8200, Hitachi technologies, Tokyo, Japan) and energy dispersive X-ray spectrometer (Hitach, Hitachi technologies, Tokyo, Japan) were used in combination to analyze the sample by SEM-EDS; Transmission electron microscope (JEOL JEM 2010FEF, Jeol, Tokyo, Japan) was used for TEM (Transmission Electron Microscope) analysis of Cs-Fe_3O_4-B_{600}.

2.3. Adsorption

To prepare the standard stock solution, ultrapure water and $Cd(NO_3)_2 \cdot 4H_2O$ were used to prepare the Cd standard stock solution. In the experiment, ultrapure water was used to dilute the standard stock solution to the required concentration.

To study the adsorption kinetics, Cd(II) solution (25 mL) with an initial pH of 5.40 and an initial concentration of 200 $mg \cdot L^{-1}$ was added to a 50 mL conical flask, and then adsorbent (0.05 g) was added to the Cd(II) solution, under the conditions of 25 °C, 200 $r \cdot min^{-1}$, using a constant temperature culture oscillator (ZHWY-2102C, Shanghai ZHICHENG analytical Instrument Manufacturing Co., Ltd., Shanghai, China) to oscillate for 1, 3, 5, 10, 20, 30, 40, 60, 90, 120, 180, 240, 300, 360, 480, 600, 720, and 1440 min. Finally, the resulting solution was passed through a 0.45 μm water filter membrane, and an atomic absorption spectrophotometer (ZEEnit 700P, Jena Analytical Instrument Co., Ltd., Thuringia, Germany) was used to determine the concentration of Cd(II) in the filtrate. At the same time, the pH of the solution was measured at the above time point. The sample loaded with Cd was washed with ultrapure water and dried at 70 °C and it was recorded as Cs-Fe_3O_4-B_{600}-Cd.

To study the adsorption isotherm, a series of Cd(II) solutions (25 mL) with an initial pH of 5.40 were added to a 50 mL conical flask, adsorbent (0.05 g) was added to the Cd(II) solution, and then under the conditions of 25 °C and 200 $r \cdot min^{-1}$, the constant-temperature culture oscillator was used to oscillate for 12 h, and the resulting solution was passed through a 0.45 μm water-based filter membrane. An atomic absorption spectrophotometer was used to determine the Cd(II) concentration in the filtrate.

To study the effect of pH on the adsorption performance of Cd(II), Cd(II) solution (25 mL) with an initial concentration of 100 $mg \cdot L^{-1}$ and an initial pH of 3–8 was added to a 50 mL conical flask, and then, adsorbent (0.05 g) was added to the Cd solution. At 25 °C and 200 $r \cdot min^{-1}$, a constant temperature incubation oscillator was used to oscillate for 30 min. Finally, the resulting solution was passed through a 0.45 μm water filter membrane, and an atomic absorption spectrophotometer was used to determine the concentration of Cd(II) in the filtrate.

2.4. Statistical Analysis

The adsorption capacity of the adsorbent for Cd(II) was calculated using the following formula:

$$q_e = \frac{(C_0 - C_t) \times V}{m} \quad (1)$$

where C_0 and C_t represent the initial concentration of Cd(II) in the solution ($mg \cdot L^{-1}$) and the concentration of Cd(II) in the solution at the adsorption time t (min) ($mg \cdot L^{-1}$), respectively; V is the volume of the solution (L); m is the mass of the adsorbent (g).

All detected data were repeated three times, and all treatments were repeated three times independently. The average value was used as the measurement result. The average value was calculated by Microsoft Excel 2010 and Origin 8.6 (OriginLab Corporation, Commonwealth of Massachusetts, America) was used for graphing.

3. Results and Discussion

3.1. Characterization of Cs-Fe_3O_4-B_{600}

Fe_3O_4 was characterized by XRD as shown in Figure S1. The XRD pattern of Fe_3O_4 has obvious diffraction apex and corresponding crystal face at 2θ = 30.091° (220), 35.443° (311), 43.074° (400), 56.964° (511), 62.553° (440). The peak shape of PDF#85-1436 is in good

agreement, indicating that its main component is Fe_3O_4, which is a pure inverse sine spinel material with a single-phase [36]. In addition, the X-ray diffraction pattern of Fe_3O_4 has a sharp diffraction apex, indicating that the self-made Fe_3O_4 has high crystallinity [37].

The magnetic hysteresis loops of Fe_3O_4 and Cs-Fe_3O_4-B_{600} are shown in Figure 1. It can be seen that the magnetic hysteresis loops of Fe_3O_4 (Figure 1a) and Cs-Fe_3O_4-B_{600} (Figure 1b) all pass through the origin, no hysteresis phenomenon occurs, and the coercivity and remanence magnetic are both zero [38]. The magnetic hysteresis loop presents an "S" shape, indicating that Fe_3O_4 and Cs-Fe_3O_4-B_{600} have superparamagnetism [15]. When the applied external field intensity is 20,000 Oe, the saturation magnetization of Fe_3O_4 and Cs-Fe_3O_4-B_{600} measured at room temperature is 66.90 and 3.30 emu·g^{-1}, respectively. The research of Huang and Tang [39] measured the saturation magnetization of pure iron bulk Fe_3O_4 as 88 emu·g^{-1}; the saturation magnetization of Fe_3O_4 synthesized by the co-precipitation method is 72.1 emu·g^{-1} [40]; the saturation magnetization of Fe_3O_4 prepared in a spiral microreactor by co-precipitation method is 53 emu·g^{-1} [15] and the above research results are similar to the measured values in this experiment. The significant decrease in saturation magnetization of Cs-Fe_3O_4-B_{600} (as low as 3.30 emu·g^{-1}) proves the successful synthesis of composite materials [41]. At the same time, we can see from the embedded picture (2) of Figure 1b that Cs-Fe_3O_4-B_{600} can be collected on the surface of the liquid by the magnet, and the liquid becomes clear. That is, although the saturation magnetization of the composite material is significantly lower than that of Fe_3O_4, it still has magnetic responsiveness and can achieve solid–liquid separation. The magnetic biochar prepared by Yuan et al. [42] by hydrothermal carbonization has strong ferromagnetism, the coercivity and remanence are 0.0 Oe and 0.0 emu·g^{-1}, respectively, and the saturation magnetization reaches 16.7 emu·g^{-1}. When the magnet is close to the aqueous solution containing magnetic biochar, the biochar particles are immediately attached to the bottle wall near the magnet, and the water becomes transparent at the same time, which is conducive to the recovery and reuse of biochar as an adsorbent.

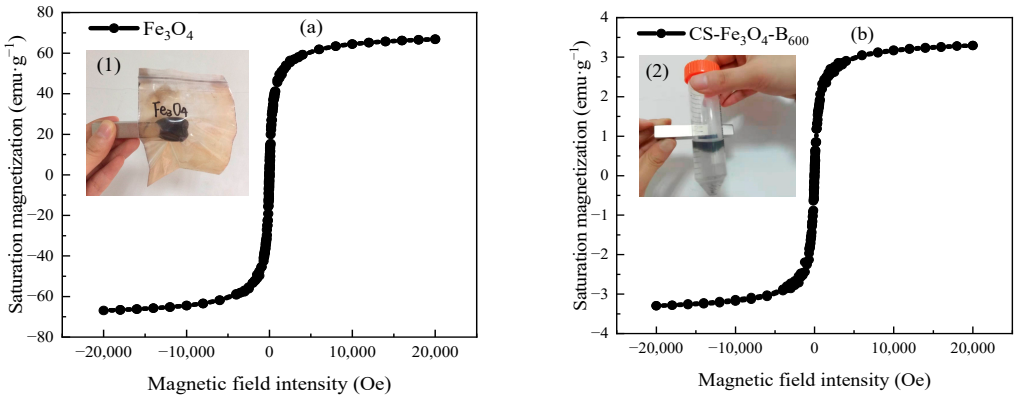

Figure 1. Hysteresis loop of Fe_3O_4 (**a**) and Cs-Fe_3O_4-B_{600} (**b**). Note: (**a**) shows the magnetism of Fe_3O_4 and (**b**) exhibits the magnetic separation of Cs-Fe_3O_4-B_{600} with a hand magnet.

The pore structures of B_{600} and Cs-Fe_3O4-B_{600} were characterized by N_2 adsorption method. It can be seen from Figure 2a that the N_2 adsorption–desorption isotherm of B_{600} belongs to a typical type IV curve, and there is an obvious H3 hysteresis loop in the range of P/P_0 = 0.2–0.9, indicating that the material belongs to mesoporous material. The N_2 adsorption–desorption isotherms of Cs-Fe_3O_4-B_{600} are a typical IV curve, and the obvious H3 hysteresis loop appeared in the range of P/P_0 = 0.6–0.9. It is generally believed that the H3 hysteresis loop is caused by the slit pores formed by the accumulation of sheet shaped particles [43], and the adsorption is the coagulation capillary effect of the mesopores [44]. According to the IUPAC pore size classification, Figure 2b shows that Cs-Fe_3O_4-B_{600} is mainly mesopores (2–50 μm). The pore volume and pore diameter measured by the BJH equation is 0.047 $cm^3 \cdot g^{-1}$, 9.764 nm, and the specific surface area measured by BET is 19.287 $m^2 \cdot g^{-1}$. B_{600} contains a large number of mesopores and macropores. The

pore volume, pore diameter, and specific surface area are 0.014 $cm^3 \cdot g^{-1}$, 19.97 nm, and 2.47 $m^2 \cdot g^{-1}$, respectively. By comparison, the composite material has a large pore volume, high specific surface area, and small pore diameter. The disappearance of the macropores of the composite material may be caused by the blockage of the macropores caused by the attachment of chitosan and Fe_3O_4 to the surface of the fish bone char. In addition, after modification, the specific surface area of biochar is greatly increased, providing more adsorption sites [45]. After the biochar prepared by Du et al. [46] was modified by Fe_3O_4, its specific surface area increased from 117.595 to 145.963 $m^2 \cdot g^{-1}$, and its pore volume increased from 0.05256 to 0.06549 $cm^3 \cdot g^{-1}$. After the rice husk biochar prepared by Zhang et al. [47] was modified with Fe_3O_4, its specific surface area and pore volume increased by 99.88 $m^2 \cdot g^{-1}$ and 0.238 $cm^3 \cdot g^{-1}$, respectively; for the Fe_3O_4 modified biochar prepared by Wang et al. [48], when the Fe^{2+} concentration increased to 0.4 $mol \cdot L^{-1}$, the specific surface area of the biochar increased significantly from 1.856 to 16.223 $m^2 \cdot g^{-1}$, and the pore volume increased from 0.011 to 0.064 $cm^3 \cdot g^{-1}$. The increases in specific surface area, pore volume, and pore size of the Fe_3O_4 modified biochar prepared in the above study are similar to this experimental study.

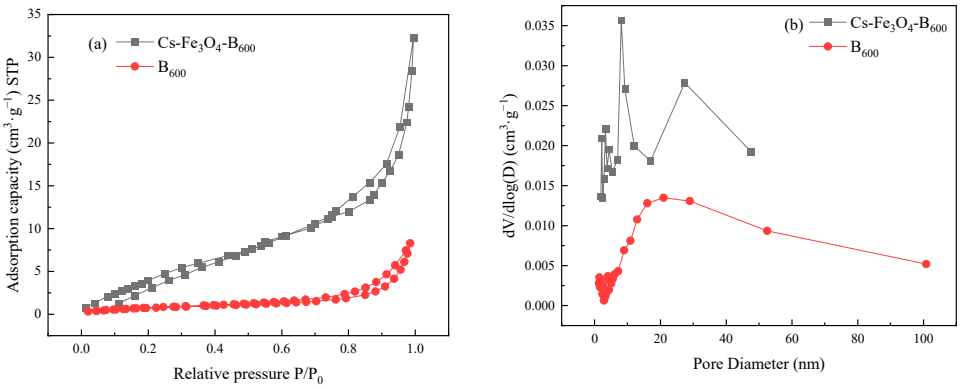

Figure 2. (**a**) N_2 adsorption–desorption isotherms and (**b**) pore size distribution (BJH) of B_{600} and Cs-Fe_3O_4-B_{600}. Note: STP means standard temperature and pressure.

3.2. The Performance of Cd(II) Adsorption on Cs-Fe_3O_4-B_{600}

3.2.1. Adsorption Kinetic Characteristics

Figure 3 shows the changing trend of Cd(II) adsorption capacity of B_{600} and Cs-Fe_3O_4-B_{600} with the continuation of the reaction time. We can see that Cs-Fe_3O_4-B_{600} more easily to reaches adsorption equilibrium than B_{600}, and it only takes 3 min. Li et al. [49] prepared nano-magnetic calcium dihydrogen phosphate and used it for the removal of Cd(II). Studies have shown that the process is a fast adsorption process, and it only takes 1 min to reach the adsorption equilibrium, involving surface adsorption, electrostatic interaction, ion exchange, complexation, and chelation [49]. In addition, the removal of As(V) by magnetite-modified water hyacinth biochar requires 5 min to reach the adsorption equilibrium [44]; the removal of Cd(II) and Pb(II) by Fe_3O_4/bentonite composite takes 30 min to reach equilibrium; the removal of Co(II), Cd(II), and Pb(II) by magnetic camel bone char takes 120 min to reach equilibrium [50]. The removal of Cd(II) by unmodified B_{600} takes 540 min to reach equilibrium (Figure 3a). In contrast, the composite adsorbent Cs-Fe_3O_4-B_{600} prepared in this experiment has certain advantages in achieving extremely fast adsorption of heavy metals.

The pseudo-first-order kinetics model (Equation (2)) and pseudo-second-order kinetics model (Equation (3)) were used to fit the obtained data. The relevant parameters obtained during the fitting process are shown in Table 1.

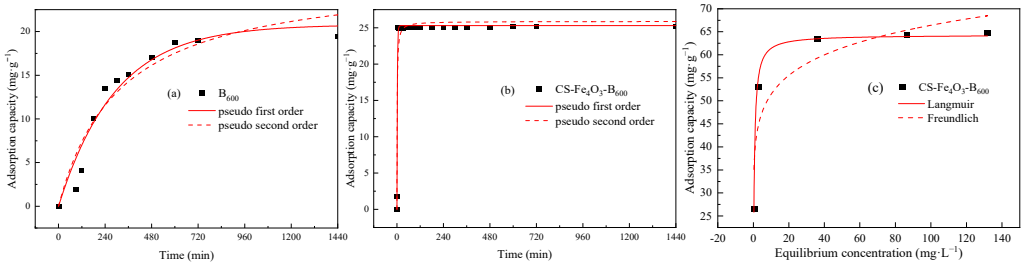

Figure 3. Fitting of kinetics of Cd(II) on B_{600} (**a**) and Cs-Fe_3O_4-B_{600} (**b**) and isotherm fitting of Cd(II) on Cs-Fe_3O_4-B_{600} (**c**).

Table 1. Pseudo-first-order and pseudo-second-order kinetics models for Cd(II) adsorption on B_{600} and Cs-Fe_3O_4-B_{600}.

Materials	C_0 (mg·L^{-1})	q_e, exp (mg·g^{-1})	Pseudo-First-Order Kinetics Model			Pseudo-Second-Order Kinetics Model		
			q_e, cal (mg·g^{-1})	k_1 (1·min^{-1})	R^2	q_e, cal (mg·g^{-1})	k_2 (g·mg^{-1}·min^{-1})	R^2
B_{600}	150	19.487	20.792	0.0034	0.9385	26.696	0.00001	0.9081
Cs-Fe_3O_4-B_{600}	150	25.134	25.284	0.4825	0.8989	25.871	0.0302	0.8305

The pseudo-first-order equation is expressed as:

$$\frac{dq_t}{dt} = k_1(q_e - q_t) \quad (2)$$

The pseudo-second-order equation is expressed as:

$$\frac{dq_t}{dt} = k_1(q_e - q_t)^2 \quad (3)$$

where q_e is the amount of Cd(II) adsorbed per unit mass of shell powder in adsorption equilibrium, mg·g^{-1}; q_t is the amount of Cd(II) absorbed per unit mass of shell powder at time t, mg·g^{-1}; t: adsorption time (min); k_1 is the rate constant, min^{-1}; k_2 is the pseudo-second-order rate constant, g·mg^{-1}·min^{-1}.

It can be seen from Table 1 that the adsorption of Cd(II) by Cs-Fe_3O_4-B_{600} is more in line with the pseudo-second-order kinetics model, and the correlation coefficient can reach 0.8989. The q_e, cal (25.284 mg·g^{-1}) obtained by the pseudo-second-order kinetics model fitting is closer to the experimental adsorption quantity q_e, exp (25.134 mg·g^{-1}). The pseudo-second-order kinetics model believes that the rate control step in the adsorption process is chemical adsorption, that is, in the adsorption process, through the covalent force and ion exchange between the adsorbent and the adsorbate, electrons are exchanged and shared, thereby forming chemical bonds [51,52].

3.2.2. Adsorption Isotherm Characteristics

Cs-Fe_3O_4-B_{600} was used to adsorb Cd(II) with different initial concentrations. After the adsorption equilibrium was reached, the adsorption amount was calculated. The obtained data were fitted with the Langmuir adsorption isotherm model (Equation (4)) and Freundlich adsorption isotherm model (Equation (5)). The fitting results are shown in Figure 3c, and the relevant parameters in the fitting process are shown in Table 2.

$$q_e = \frac{Q_m K_L C_e}{1 + K_L C_e} \quad (4)$$

$$q_e = K_F C_e^{\frac{1}{n}} \quad (5)$$

where q_e is the equilibrium adsorption capacity, mg·g^{-1}; Q_m is the adsorption constant; C_e is equilibrium concentration, mg·L^{-1}; K_L is adsorption parameters, L·mg^{-1}; K_F is adsorption capacity, mg·g^{-1}(L·mg^{-1})$^{1/n}$.

Table 2. Langmuir and Freundlich isotherm models for Cd(II) adsorption on Cs-Fe_3O_4-B_{600} and B_{600}.

Adsorption Isotherm Model	Parameter	Adsorbent Cs-Fe_3O_4-B_{600}	Adsorbent B_{600}
Langmuir	q_m (mg·g^{-1})	64.310	37.799
	K_L (L·mg^{-1})	2.0890	0.0591
	R^2	0.8653	0.9892
Freundlich	K_F (mg·g^{-1}(L·g^{-1})$^{1/n}$)	39.804	7.4522
	n	8.9967	3.1546
	R^2	0.7704	0.9362

The correlation coefficient R^2 of Langmuir equation fitting is 0.8653, which is higher than the correlation coefficient of the Freundlich equation of 0.7704. Therefore, compared with the Freundlich model, the adsorption of Cd(II) by Cs-Fe_3O_4-B_{600} is more in line with the Langmuir isotherm adsorption model. This model assumes that there is no interaction between the adsorbed molecules, that is, once Cd(II) occupies a certain adsorption site, the site will not undergo further adsorption. Therefore, it is assumed that the adsorption process is a single-layer adsorption and there is a saturated adsorption capacity. Cs-Fe_3O_4-B_{600} has abundant available adsorption sites on the surface at the beginning of the adsorption process. As the adsorption process continues, the number of available adsorption sites of Cs-Fe_3O_4-B_{600} decreases, so the adsorption amount slowly rises until it remains unchanged [53]. The saturated adsorption capacity q_m obtained in this study is 64.310 mg·g^{-1}, which is far greater than the saturated adsorption capacity of unmodified fish bone char B_{600} (37.799 mg·g^{-1}, Table 2). Other studies have shown that the saturated adsorption capacity of Fe_3O_4/bentonite composite for Pb(II) can reach 81.5 mg·g^{-1}, which is 10.7 mg·g^{-1} more than that of unmagnetic modified bentonite [54]. The saturated adsorption capacity of magnetic corn stover biochar for Cd(II) in water can reach 43.45 mg·g^{-1}, which is greater than the 25.31 mg·g^{-1} of unmodified corn stover biochar [31]. Reza et al. [35] studied the removal of As(V) by magnetically modified bone char coated with chitosan. The results showed that the modified material is at 600 cm^{-1}. Fe-O functional groups can be observed, the adsorption of arsenic is mainly monolayer adsorption, and the saturated adsorption capacity can reach 112,000 mg·g^{-1}. In addition, R_L is the separation factor. For the Langmuir adsorption isotherm model, it can be calculated by formula 6 to determine whether the reaction is favorable adsorption. In this experiment, $R_L < 1$ indicates that the adsorption process is favorable adsorption.

$$R_L = \frac{1}{1 + K_L C_e} \quad (6)$$

3.2.3. Influence of pH on Cd(II) Adsorption

The relationship between the adsorption capacity of Cs-Fe_3O_4-B_{600} and the initial pH value is shown in Figure 4. Studies have shown that in the range of pH = 3–7 (when the acidity is low) Fe ions will not be generated in the system [31]; at the same time, at pH < 8, Cd mainly exists in the state of Cd(II). When the adsorbent dosage is 2 g·L^{-1} and the initial concentration is 100 mg·L^{-1}, the adsorption capacity will increase significantly between pH = 3–5 and then slowly increase with the increase of pH. The adsorption capacity of Cs-Fe_3O_4-B_{600} varies from 46.08 to 48.64 mg·g^{-1} and 48.64 to 50.22 mg·g^{-1}. The total increase in adsorption capacity is 4.14 mg·g^{-1}, indicating that pH has a weak effect on the adsorption of Cd(II) on Cs-Fe_3O_4-B_{600}. The trend of the relationship curve between the

adsorption capacity of glutamic acid coupled chitosan modified activated carbon on Cd(II) and the initial pH value is consistent with this study [55].

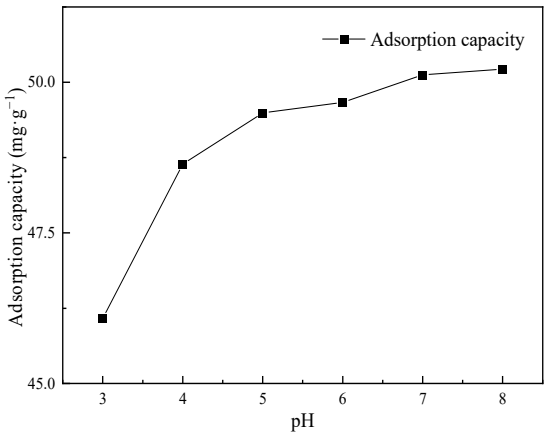

Figure 4. Effect of initial pH values on the adsorption of Cd(II) on Cs-Fe_3O_4-B_{600}.

Cs and B_{600} may combine with Fe_3O_4 through the surface hydroxyl group and the intermediate oxygen (-O-) in the carboxyl functional group. The involved process is shown in formula 7 and formula 8 [56]. The adsorption of Cd(II) by Cs-Fe_3O_4-B_{600} mainly includes ion exchange, surface complexation and precipitation of partially exposed to Cs-coated outer fish bone char, complexation of heavy metals with amino groups on Cs [57], and cations of composite materials specific adsorption, electrostatic adsorption. In addition, it may also include the ion exchange between isomorphic Cd(II) and Fe_3O_4 to produce $CdFe_2O_4$ [56]. When the pH of the solution is low, there is competitive adsorption of H^+ and Cd(II); at the same time, the amino groups on the surface of Cs-Fe_3O_4-B_{600} are protonated in the presence of a large amount of H^+ to form NH^{3+}. The electrostatic repulsion between NH^{3+} and Cd(II) also makes the adsorption capacity low. With the increase of pH, the amino groups on the surface of chitosan are released, and the complexing ability of Cd(II) increases [58].

$$R - OH + Fe_3O_4 \rightarrow R - O - Fe_3O_4 \quad (7)$$

$$R - COOH + Fe_3O_4 \rightarrow R - COO - Fe_3O_4 \quad (8)$$

3.3. Characterization of Cs-Fe_3O_4-B_{600} before and after Adsorption

The FTIR spectra of Fe_3O_4, B_{600}, B_{600}-Cd, Cs-Fe_3O_4-B_{600}, and Cs-Fe_3O_4-B_{600}-Cd are shown in Figure 5. Fe_3O_4 has three prominent absorption peaks at 578, 1629, and 3405 cm^{-1}. The peak at 550–580 cm^{-1} is considered to be the characteristic peak of Fe_3O_4, which is caused by the stretching vibration of Fe-O [59]. Compared with the FTIR spectrum of B_{600}, Cs-Fe_3O_4-B_{600} and Cs-Fe_3O_4-B_{600}-Cd have new absorption peaks at 551 and 562 cm^{-1}, respectively, which are believed to be caused by Fe_3O_4 in the composite material. The prominent absorption peaks of B_{600} material exist at 1090, 1460, 2924, and 2428 cm^{-1}, representing PO_4^{3-}, C=O, -CH_2, and -OH, respectively. The coating effect of Cs may cause the weakening of PO_4^{3-} strength in Cs-Fe_3O_4-B_{600}. In addition, the absorption peaks of Cs-Fe_3O_4-B_{600} at 1410 and 1580 cm^{-1} are believed to be caused by the symmetrical variable-angle vibration of the -CH_3 and amide II bands in Cs [60], which are based on Cs A slight red shift [59]. The appearance of Fe_3O_4 and Cs characteristic peaks in the Cs-Fe_3O_4-B_{600} material indicates that the material was successfully synthesized. Du et al. [30] used the co-precipitation method to prepare Fe_3O_4 magnetic biochar. The results showed that the infrared absorption peaks of C-H, C≡N, and Fe_3O_4 appeared after magnetic modification. The increase of hydroxyl, carboxyl, and other functional groups in the modification process enhances its ability to remove heavy metals through hydrogen bonding and ion exchange; the presence of aromatic functional groups can cause complexes with heavy metals; when the pH is high, heavy metals form hydroxyl complexes and magnetic materials can adsorb

heavy metals through electrostatic interaction [61]. According to the FTIR results before and after Cs-Fe_3O_4-B_{600} adsorption of Cd(II), it can be seen that there are many band shifts, indicating that a variety of functional groups participate in the adsorption process of Cd(II). There are methyl or methylene absorption peaks at 1445 and 3034 cm^{-1}, which move from 1445 to 1417 cm^{-1} after adsorption, and the carboxylic acid C=O stretching vibration peak at 1579 cm^{-1}, which moves to 1608 cm^{-1}. It shows that there are a large number of carboxyl groups and hydroxyl groups in the molecular structure of Cs-Fe_3O_4-B_{600}. The hydroxyl groups and carboxyl groups can undergo ion exchange and complexation reactions with Cd(II). In this study, comparing the infrared spectra of Cs-Fe_3O_4-B_{600} and Cs-Fe_3O_4-B_{600}-Cd, it can be found that the intensity of the absorption peak caused by the amide II band is weakened, which may be caused by the amino group complexing Cd(II). The research of Muzzarelli [57] showed that the amino group of Cs has a complexing effect on Cd(II).

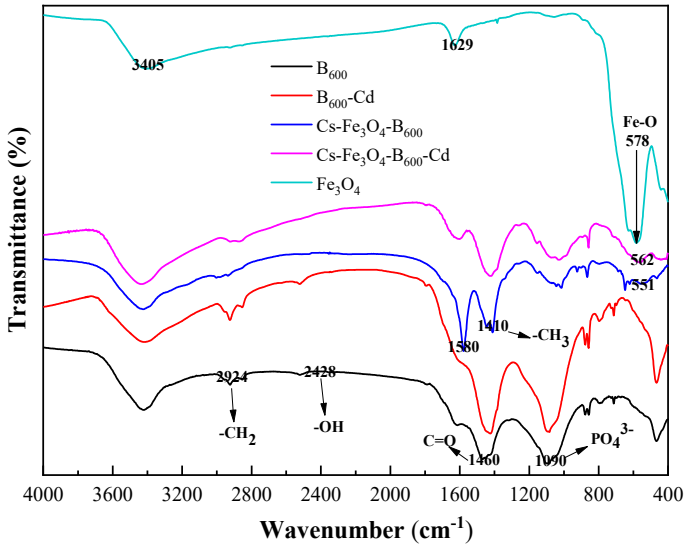

Figure 5. FTIR curves of Fe_3O_4, B_{600}, B_{600}-Cd, Cs-Fe_3O_4-B_{600}, and Cs-Fe_3O_4-B_{600}-Cd.

The SEM images of Fe_3O_4, Cs-Fe_3O_4-B_{600}, and Cs-Fe_3O_4-B_{600}-Cd are presented in Figure 6. The Fe_3O_4 prepared in this experiment has spherical particles with a particle size of about 20–200 μm (Figure 6b), which is in contrast to Deng [62] and Peng [63] and other research conclusions are consistent. In addition, the surface of Fe_3O_4 particles is rough and coated with a large number of amorphous microspheres [64]. The TEM Figure 6f of Fe_3O_4 shows that most of the microspheres are intact. The SEM images of B_{600} (Figure 6a) show that there are cracks and gullies on the surface of B_{600}, with a large number of mesopores and macropores. Comparing the SEM images of Cs-Fe_3O_4-B_{600} (Figure 6c), it can be found that Cs wrapped B_{600} and Fe_3O_4, blocked the macropores of B_{600}, and formed a rough outer surface structure. This conclusion is consistent with the BJH pore size distribution of Cs-Fe_3O_4-B_{600}. Figure 6g shows that the spherical particles are coated. Figure 6d can clearly observe the spherical Fe_3O_4 particles attached to the bone char in Cs-Fe_3O_4-B_{600}-Cd, that is, the spindle-shaped Cd(II) attached to it. The transmission electron microscope can also observe the obvious Cd spindle structure, showing that Cd(II) is adsorbed on it. The EDS analysis of Cs-Fe_3O_4-B_{600}-Cd showed that after adsorption, Cs-Fe_3O_4-B_{600} detected 20.65 wt.% Cd, which confirmed the consistency of SEM and TEM analysis results.

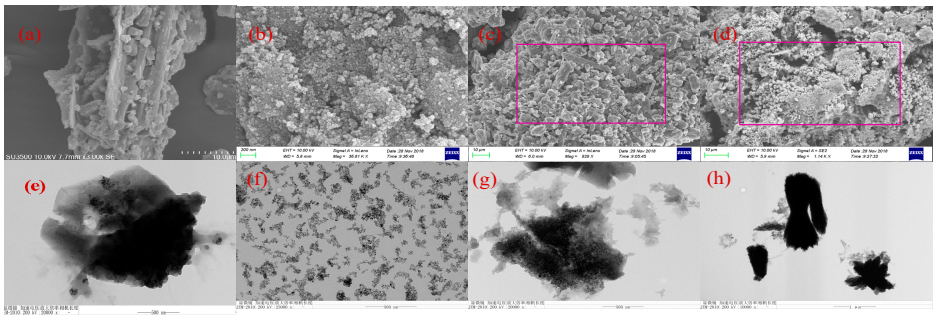

Element （wt.%）	Ca	Fe	Na	C	O	Si	Others	Cd
Cs-Fe_3O_4-B_{600}	2.88	16.91	0.62	36.22	39.22	2.82	1.33	ND
Cs-Fe_3O_4-B_{600}-Cd	1.45	14.57	0.43	24.81	35.12	2.01	0.96	20.65

Figure 6. SEM and TEM images of B_{600} (**a**,**e**), Fe_3O_4 (**b**,**f**), Cs-Fe_3O_4-B_{600} (**c**,**g**), and Cs-Fe_3O_4-B_{600}-Cd (**d**,**h**). Note: the table shows the element compositions of Cs-Fe_3O_4-B_{600} (**c**) and Cs-Fe_3O_4-B_{600}-Cd (**d**).

4. Conclusions

Cs-Fe_3O_4-B_{600} was successfully fabricated, modified with chitosan and Fe_3O_4 based on B_{600}. The kinetic data of Cs-Fe_3O_4-B_{600} are in the best agreement with the pseudo-second-order model, and the maximum Cd^{2+} adsorption capacity by Cs-Fe_3O_4-B_{600} is 25.284 $mg \cdot g^{-1}$ in solution when the initial Cd^{2+} concentration is 150 $mg \cdot L^{-1}$. Adsorption isotherms are in better accordance with Langmuir models. Thermodynamic analysis explained that the adsorption process, which was monolayer adsorption, was a favorable adsorption. The saturated adsorption capacity of Cs-Fe_3O_4-B_{600} for Cd(II) increased from 37.799 $mg \cdot g^{-1}$ before unmodified to 64.31 $mg \cdot g^{-1}$. Cs-Fe_3O_4-B_{600} was analyzed using different techniques (SEM-EDS, TEM, BET, FTIR, and XRD). The resulting Cs-Fe_3O_4-B_{600} composites manifested tremendous physicochemical properties such as the appearance of amino functional groups, larger specific surface area, and larger pore volume. Cd(II) successfully adsorbed onto Cs-Fe_3O_4-B_{600} because of the amino complexation, ion exchange, precipitation, cation-specific adsorption, and electrostatic adsorption. In conclusion, applying Cs-Fe_3O_4-B_{600} could be a low-cost, fast, and efficient solution for the removal of Cd(II) in water.

Supplementary Materials: The following supporting information can be downloaded at: https://www.mdpi.com/article/10.3390/ijerph19031260/s1, Figure S1: XRD pattern of Fe_3O_4.

Author Contributions: Conceptualization, W.L. and W.Y.; methodology, W.L.; software, W.Y.; validation, W.Y.; formal analysis, W.Y.; investigation, W.Y.; resources, W.L.; data curation, W.L.; writing—original draft preparation, W.Y.; writing—review and editing, W.Y.; visualization, T.S.; supervision, T.S. and W.Y.; project administration, Y.X.; funding acquisition, Y.S. All authors have read and agreed to the published version of the manuscript.

Funding: This research was funded by the National Natural Science Foundation of China (31971525), the National Key Research and Development Program of China (2018YFD0800300).

Institutional Review Board Statement: Not applicable.

Informed Consent Statement: Not applicable.

Data Availability Statement: The data presented in this study are available on reasonable request from the corresponding author. The data are not publicly available due to privacy or ethical considerations.

Acknowledgments: This research was funded by the National Natural Science Foundation of China (31971525), the National Key Research and Development Program of China (2018YFD0800300).

Conflicts of Interest: The authors declare no conflict of interest.

References

1. Li, C.; Huang, Q.; Zhang, H.; Wang, Q.; Xue, R.; Guo, G.; Hu, J.; Li, T.; Wang, J.; Hu, S. Characterization of Biochars Produced by Co-Pyrolysis of Hami Melon (Cantaloupes) Straw Mixed with Polypropylene and Their Adsorption Properties of Cadmium. *Int. J. Environ. Res. Public Health* **2021**, *18*, 11413. [CrossRef] [PubMed]
2. Zhao, X.; Wang, M.; Wang, H.; Tang, D.; Huang, J.; Sun, Y. Study on the Remediation of Cd Pollution by the Biomineralization of Urease-Producing Bacteria. *Int. J. Environ. Res. Public Health* **2019**, *16*, 268. [CrossRef] [PubMed]
3. Chen, H.; Yang, X.; Wang, P.; Wang, Z.; Li, M.; Zhao, F. Dietary cadmium intake from rice and vegetables and potential health risk: A case study in Xiangtan, southern China. *Sci. Total Environ.* **2018**, *639*, 271–277. [CrossRef] [PubMed]
4. Zhuang, Z.; Nio-Savala, A.G.; Mi, Z.D.; Wan, Y.N.; Fangmeier, A. Cadmium accumulation in wheat and maize grains from China: Interaction of soil properties, novel enrichment models and soil thresholds. *Environ. Pollut.* **2021**, *275*, 116–623. [CrossRef] [PubMed]
5. Wang, H.; Li, W.; Zhu, C.; Tang, X. Analysis of Heavy Metal Pollution in Cultivated Land of Different Quality Grades in Yangtze River Delta of China. *Int. J. Environ. Res. Public Health* **2021**, *18*, 9876. [CrossRef] [PubMed]
6. Chen, D.; Wang, X.; Wang, X.; Feng, K.; Su, J.; Dong, J. The mechanism of cadmium sorption by sulphur-modified wheat straw biochar and its application cadmium-contaminated soil. *Sci. Total Environ.* **2020**, *714*, 136550. [CrossRef] [PubMed]
7. Coutand, M.; Deydie, E.; Cyr, M.; Mouchet, F.; Gauthier, L.; Guilet, R.; Savaete, L.B.; Cren, S.; Clastres, P. Evaluation of laboratory and industrial meat and bone meal combustion residue as cadmium immobilizing material for remediation of polluted aqueous solutions: "Chemical and ecotoxicological studies". *J. Hazard. Mater.* **2009**, *166*, 945–953. [CrossRef]
8. Gupta, V.K.; Carrott, P.J.M.; Ribeiro Carrott, M.M.L.; Suhas. Low-Cost Adsorbents: Growing Approach to Wastewater Treatment—A Review. *Crit. Rev. Environ. Sci. Technol.* **2009**, *39*, 783–842. [CrossRef]
9. Merrikhpour, H.; Jalali, M. Waste calcite sludge as an adsorbent for the removal of cadmium, copper, lead, and zinc from aqueous solutions. *Clean Technol. Environ. Policy* **2012**, *14*, 845–855. [CrossRef]
10. Nie, F.; Liu, R.; Zhou, Y.; Liu, Z. Research Advances of Lignocellulosic Wastes of the Adsorption of Metal Ions in Wastewater. *Technol. Water Treat.* **2016**, *42*, 12–19.
11. Reynel-Avila, H.E.; Mendoza-Castillo, D.I.; Bonilla-Petriciolet, A. Relevance of anionic dye properties on water decolorization performance using bone char: Adsorption kinetics, isotherms and breakthrough curves. *J. Mol. Liq.* **2016**, *219*, 425–434. [CrossRef]
12. Xu, Y.; Schwartz, F.W.; Traina, S.J. Sorption of Zn^{2+} and Cd^{2+} on hydroxyapatite surfaces. *Environ. Sci. Technol.* **1994**, *28*, 1472–1480. [CrossRef] [PubMed]
13. Dimović, S.; Smičiklas, I.; Plećaš, I.; Antonović, D.; Mitrić, M. Comparative study of differently treated animal bones for Co^{2+} removal. *J. Hazard. Mater.* **2009**, *164*, 279–287. [CrossRef] [PubMed]
14. Kizilkaya, B.; Tekinay, A.A.; Dilgin, Y. Adsorption and removal of Cu (II) ions from aqueous solution using pretreated fish bones. *Desalination* **2010**, *264*, 37–47. [CrossRef]
15. Wang, D.; Iqbal, M.; Zhu, M.Q. Synthesis of Fe_3O_4 Magnetic Nanoparticles in a Helical Microreactor. *Key Eng. Mater.* **2020**, *842*, 174–181. [CrossRef]
16. Liu, J.; Huang, X.; Liu, J.; Wang, W.; Zhang, W.; Dong, F. Adsorption of arsenic(V) on bone char: Batch, column and modeling studies. *Environ. Earth Sci.* **2014**, *842*, 174–181. [CrossRef]
17. Moreno, J.C.; Gómez, R.; Giraldo, L. Removal of Mn, Fe, Ni and Cu Ions from Wastewater Using Cow Bone Charcoal. *Materials* **2010**, *3*, 452–466. [CrossRef]
18. Sneddon, I.R.; Orueetxebarria, M.; Hodson, M.E.; Schofield, P.F.; Valsami-Jones, E. Use of bone meal amendments to immobilise Pb, Zn and Cd in soil: A leaching column study. *Environ. Pollut.* **2006**, *144*, 816–825. [CrossRef]
19. Qin, R.; Li, F.; Chen, M.; Jiang, W. Preparation of chitosan-ethylenediaminetetraacetate-enwrapped magnetic $CoFe_2O_4$ nanoparticles via zero-length emulsion crosslinking method. *Appl. Surf. Sci.* **2009**, *256*, 27–32. [CrossRef]
20. Srivastava, M.; Ojha, A.K.; Chaubey, S.; Singh, J. In-situ synthesis of magnetic ($NiFe_2O_4$/CuO/FeO) nanocomposites. *J. Solid State Chem.* **2010**, *183*, 2669–2674. [CrossRef]
21. Covaliu, C.I.; Berger, D.; Matei, C.; Diamandescu, L.; Vasile, E.; Cristea, C.; Ionita, V.; Iovu, H. Magnetic nanoparticles coated with polysaccharide polymers for potential biomedical applications. *J. Nanopart. Res.* **2011**, *13*, 6169–6180. [CrossRef]
22. Singh, J.; Srivastava, M.; Dutta, J.; Dutta, P.K. Preparation and properties of hybrid monodispersed magnetic α-Fe_2O_3 based chitosan nanocomposite film for industrial and biomedical applications. *Int. J. Biol. Macromol.* **2011**, *48*, 170–176. [CrossRef] [PubMed]
23. Lin, Y.; Yao, W.; Cheng, Y.; Qian, H.; Wang, X.; Ding, Y.; Wu, W.; Jiang, X. Multifold enhanced T2 relaxation of $ZnFe_2O_4$ nanoparticles by jamming them inside chitosan nanospheres. *J. Mater. Chem.* **2012**, *22*, 5684–5693. [CrossRef]
24. Zhang, M.; Gao, B.; Varnoosfaderani, S.; Hebard, A.; Yao, Y.; Inyang, M. Preparation and characterization of a novel magnetic biochar for arsenic removal. *Bioresour. Technol.* **2013**, *130*, 457–462. [CrossRef] [PubMed]
25. Liu, X.; Liu, M.; Zhang, L. Co-adsorption and sequential adsorption of the co-existence four heavy metal ions and three fluoroquinolones on the functionalized ferromagnetic 3D $NiFe_2O_4$ porous hollow microsphere. *J. Colloid Interface Sci.* **2018**, *511*, 135–144. [CrossRef]
26. Gong, Y.; Gai, L.; Tang, J.; Fu, J.; Wang, Q.; Zeng, E.Y. Reduction of Cr(VI) in simulated groundwater by FeS-coated iron magnetic nanoparticles. *Sci. Total Environ.* **2017**, *595*, 743–751. [CrossRef]

27. Shekari, H.; Sayadi, M.H.; Rezaei, M.R.; Allahresani, A. Synthesis of nickel ferrite/titanium oxide magnetic nanocomposite and its use to remove hexavalent chromium from aqueous solutions. *Surf. Interfaces* **2017**, *8*, 199–205. [CrossRef]
28. Pisanic, T.R.; Blackwell, J.D.; Shubayev, V.I.; Fiñones, R.R.; Jin, S. Nanotoxicity of iron oxide nanoparticle internalization in growing neurons. *Biomaterials* **2007**, *28*, 2572–2581. [CrossRef]
29. Luo, L.; Li, Q.; Xu, Y.; Ding, Y.; Wang, X.; Deng, D.; Xu, Y. Amperometric glucose biosensor based on $NiFe_2O_4$ nanoparticles and chitosan. *Sens. Actuat. B Chem.* **2010**, *145*, 293–298. [CrossRef]
30. Du, W.Q.; Cao, W.; Zhou, H.; Yang, W.T.; Gu, J.F.; Peng, P.Q.; Zhang, P.; Liao, B.H. Optimization and the mechanismin treatment of heavy metals wastewater with magnetic biochar. *Acta Sci. Circumstantiae* **2018**, *38*, 492–500.
31. Hu, X.Y.; Chen, Y.J.; Zhang, S.S.; Wang, X.Q.; Li, C.C.; Guo, X. Cd removal from aqueous solution using magnetic biochar derived from maize straw and its recycle. *Trans. Chin. Soc. Agric. Eng.* **2018**, *34*, 208–218.
32. Jiangxin, X.; Qintie, L.; Xiaosheng, Y.; Guangcai, Y. Removal of Cd from aqueous solution by chitosan coated MgO-biochar and its in-situ remediation of Cd-contaminated soil. *Environ. Res.* **2021**, *195*, 110650.
33. Kumuduni, N.P.; Sok, K.; Avanthi, D.I.; Yohey, H.; Yoon, -E.C.; Raj, M.; Binoy, S.; Yong, S.O. Fe(III) loaded chitosan-biochar composite fibers for the removal of phosphate from water. *J. Hazard. Mater.* **2021**, *415*, 125464.
34. Yuehui, T.; Xirui, W.; Xue, N.; Le, W.; Ting, Z.; Huimin, S.; Nong, W.; Xianqiang, Y. Efficient removal of Cd (II) from aqueous solution by chitosan modified kiwi branch biochar. *Chemosphere* **2022**, *289*, 133251.
35. Reza, D.; Safari, M.; Maleki, A.; Rezaee, R.; Shahmoradi, B.; Shahmohammadi, S.; Ghahramani, E. Decontamination of arsenic (V)-contained liquid phase utilizing Fe_3O_4/bone char nanocomposite encapsulated in chitosan biopolymer. *Environ. Sci. Pollut. Res.* **2017**, *24*, 15157–15166.
36. Mohammadi, A.; Barikani, M. Synthesis and characterization of superparamagnetic Fe_3O_4 nanoparticles coated with thiodiglycol. *Mater. Charact.* **2014**, *90*, 88–93. [CrossRef]
37. Hu, B.; Wu, L.; Ou, M.; Wang, X.; Tang, Y. Sorption Studies of Chromium(VI) onto Cerium/Ferroferric Oxide Composites. *J. Inorg. Organomet. Polym. Mater.* **2021**, *31*, 2627–2637. [CrossRef]
38. Lan, F.; Liu, K.X.; Jiang, W.; Zeng, X.B.; Wu, Y.; Gu, Z.W. Facile synthesis of monodisperse superparamagnetic Fe_3O_4/PMMA composite nanospheres with high magnetization. *Nanotechnology* **2011**, *22*, 225604. [CrossRef]
39. Huang, Z.; Tang, F. Preparation, structure, and magnetic properties of mesoporous magnetite hollow spheres. *J. Colloid Interface Sci.* **2005**, *281*, 432–436. [CrossRef]
40. Dirgayanti, D.S.; Koesnarpadi, S.; Hindryawati, N. Synthesis and characterization of Fe_3O_4-Activated Carbon and it's application to adsorb methylene blue. *IOP Conf. Ser. Earth Environ. Sci.* **2021**, *623*, 012070. [CrossRef]
41. Dong, S.L.; Weng, T.; Wang, X.L.; Wang, H.X.; Liu, Y.J. Preprartion and characterization of Fe_3O_4/CS@CQDs bifuntional magnetic fluorescent composite. *New Chem. Mater.* **2018**, *46*, 121–124.
42. Yuan, J.; Qian, Y.J.; Xue, G.; Zhang, Q.; LI, Q.; Liu, Z.H.; Li, X.Y. Removal of Cadmium and Lead in Water by Magnetic Carbon Prepared from Activated Sludge with Hydrothermal Carbonization. *Environ. Eng.* **2020**, *38*, 55–62.
43. Zheng, X.Q.; Miao, T.B.; Zhang, C.; Ye, X.X.; Liu, M.H. Adsorption Behavior of Cr(VI) on Aminated Cyanoethyl Lignin Adsorbent. *China Pulp Pap.* **2015**, *34*, 37–43.
44. Zhang, F.; Wang, X.; Xionghui, J.; Ma, L. Efficient arsenate removal by magnetite-modified water hyacinth biochar. *Environ. Pollut.* **2016**, *216*, 575–583. [CrossRef]
45. Cao, W.; Zhou, H.; Deng, G.Y.; Du, W.Q. Effects and mechanisms of magnetic iron supported on rice husk biochar removing Pb^{2+} in wastewater. *Chin. J. Environ. Eng.* **2017**, *11*, 1437–1444.
46. Du, C.; Song, Y.; Shi, S.; Jiang, B.; Yang, J.; Xiao, S. Preparation and characterization of a novel Fe_3O_4-graphene-biochar composite for crystal violet adsorption. *Sci. Total Environ.* **2020**, *711*, 134662. [CrossRef]
47. Zhang, J.; Zhou, H.; Gu, J.; Huang, F.; Yang, W.; Wang, S.; Yuan, T.; Liao, B. Effects of nano-Fe_3O_4-modified biochar on iron plaque formation and Cd accumulation in rice (*Oryza sativa* L.). *Environ. Pollut.* **2020**, *260*, 113970. [CrossRef]
48. Wang, J.; Chen, W.; Zhang, M.; Zhou, R.; Li, J.; Zhao, W.; Wang, L. Optimize the preparation of Fe_3O_4-modified magnetic mesoporous biochar and its removal of methyl orange in wastewater. *Environ. Monit. Assess.* **2021**, *193*, 179. [CrossRef]
49. Li, Y.J.; Yang, Z.M.; Chen, Y.C.; Huang, L.; Tang, H.Y. Adsorption, Reclaim, and Regeneration of Cd by Magnetic Calcium Dihydrogen Phosphate Nanoparticles. *Environ. Sci.* **2019**, *40*, 1849–1856.
50. Alqadami, A.A.; Khan, M.A.; Otero, M.; Siddiqui, M.R.; Jeon, B.; Batoo, K.M. A magnetic nanocomposite produced from camel bones for an efficient adsorption of toxic metals from water. *J. Clean. Prod.* **2018**, *178*, 293–304. [CrossRef]
51. Lu, S.; Gibb, S.W. Copper removal from wastewater using spent-grain as biosorbent. *Bioresour. Technol.* **2008**, *99*, 1509–1517. [CrossRef] [PubMed]
52. Tekin, N.; Şafaklı, A.; Bingöl, D. Process modeling and thermodynamics and kinetics evaluation of Basic Yellow 28 adsorption onto sepiolite. *Desalination Water Treat.* **2015**, *54*, 2023–2035. [CrossRef]
53. Zheng, L.; Gao, Y.; Du, J.; Zhang, W.; Huang, Y.; Zhao, Q.; Duan, L.; Liu, Y.; Naidu, R.; Pan, X. Single and Binary Adsorption Behaviour and Mechanisms of Cd^{2+}, Cu^{2+} and Ni^{2+} onto Modified Biochar in Aqueous Solutions. *Processes* **2021**, *9*, 1829. [CrossRef]
54. Yan, L.; Li, S.; Yu, H.; Shan, R.; Du, B.; Liu, T. Facile solvothermal synthesis of Fe_3O_4/bentonite for efficient removal of heavy metals from aqueous solution. *Powder Technol.* **2016**, *301*, 632–640. [CrossRef]

55. Xiao, S.G.; Liu, Y.X.; Yu, X.J.; Jin, G.Z.; Xiao, X.X. Adsorption and Desorption of Cd^{2+} on Activated Carbon Modified by Glutamate Coupling Chitosan. *Inn. Mong. Ind.* **2015**, *41*, 6–8.
56. Tan, Z.; Wang, Y.; Kasiulienė, A.; Huang, C.; Ai, P. Cadmium removal potential by rice straw-derived magnetic biochar. *Clean Technol. Environ. Policy* **2017**, *19*, 761–774. [CrossRef]
57. Muzzarelli, R.A.A. Chitosan composites with inorganics, morphogenetic proteins and stem cells, for bone regeneration. *Carbohyd. Polym.* **2011**, *83*, 1433–1445. [CrossRef]
58. Cheng, S.S.; Yang, X.H.; Zhang, C.H.; Xie, W.C.; Qin, X.M.; Lu, H.Y. Adsorption of Cd^{2+} and Pb^{2+} by Chitosan. *J. Fish. China* **2011**, *35*, 410–416.
59. Yan, S.Q.; Zhang, H.C.; Fu, H.; Pan, Y.J. Preparation and adsorption properties of magnetic chitosan adsorbent for heavy metals. *J. Shanghai Ocean. Univ.* **2018**, *27*, 739–747.
60. Wang, C.X.; Wang, L.X.; Yang, W.L. Preparation and characterization of functional inorganic/organic composite microspheres via electrostatic interaction. *J. Colloid Interface Sci.* **2009**, *333*, 749–756. [CrossRef]
61. Ghafoor, S.; Ata, S. Synthesis of carboxyl-modified Fe_3O_4@SiO_2 nanoparticles and their utilization for the remediation of cadmium and nickel from aqueous solution. *J. Chil. Chem. Soc.* **2017**, *62*, 3588–3592. [CrossRef]
62. Deng, H.; Li, X.L.; Peng, Q.; Wang, X.; Chen, J.P.; Li, Y.D. Monodisperse magnetic single-crystal ferrite microspheres. *Angew. Chem. Int. Ed.* **2010**, *44*, 2782–2785. [CrossRef] [PubMed]
63. Peng, H.X.; Liu, G.X.; Dong, X.T.; Wang, J.X.; Xu, J.; Yu, W.S. Preparation and characteristics of Fe_3O_4 @YVO_4:Eu^{3+} bifunctional magnetic-luminescent nanocomposites. *J. Alloys Compd.* **2011**, *509*, 6930–6934. [CrossRef]
64. Shang, J.; Zhao, J. Effect of chitosan modification on Pb(II) and Cd(II) adsorption by magnetic Fe_3O_4. *Environ. Pollut. Control* **2017**, *39*, 746–751.